Protein Science (1996), 5:2391–2398. Cambridge University Press. Printed in the USA.

Comparison of the NMR and X-ray structures of the HIV-1 matrix protein: Evidence for conformational changes during viral assembly

MICHAEL A. MASSIAH,[1,3] DAVID WORTHYLAKE,[2] ALLYSON M. CHRISTENSEN,[2] WESLEY I. SUNDQUIST,[2] CHRISTOPHER P. HILL,[2] AND MICHAEL F. SUMMERS[1]

[1]Howard Hughes Medical Institute, and the Department of Chemistry and Biochemistry, University of Maryland Baltimore County, Baltimore, Maryland 21228

[2]Department of Biochemistry, University of Utah, Salt Lake City, Utah 84132

(RECEIVED September 9, 1996; ACCEPTED September 27, 1996)

Abstract

The three-dimensional solution- and solid-state structures of the human immunodeficiency virus type-1 (HIV-1) matrix protein have been determined recently in our laboratories by NMR and X-ray crystallographic methods (Massiah et al. 1994. *J Mol Biol 244*:198–223; Hill et al. 1996. *Proc Natl Acad Sci USA 93*:3099–3104). The matrix protein exists as a monomer in solution at low millimolar protein concentrations, but forms trimers in three different crystal lattices. Although the NMR and X-ray structures are similar, detailed comparisons have revealed an approximately 6 Å displacement of a short 3_{10} helix (Pro 66–Gly 71) located at the trimer interface. High quality electron density and nuclear Overhauser effect (NOE) data support the integrity of the X-ray and NMR models, respectively. Because matrix apparently associates with the viral membrane as a trimer, displacement of the 3_{10} helix may reflect a physiologically relevant conformational change that occurs during virion assembly and disassembly. These findings further suggest that Pro 66 and Gly 71, which bracket the 3_{10} helix, serve as "hinges" that allow the 3_{10} helix to undergo this structural reorientation.

Keywords: human immunodeficiency virus type 1; matrix protein; NMR spectroscopy; retroviral assembly; X-ray crystallography

The human immunodeficiency virus type-1 (HIV-1) genome encodes the structural Gag polyprotein (p55), which accumulates at the cell membrane during the late stages of the virus life cycle. Approximately 2,000 copies of the polyprotein assemble to form each immature virion. As these immature virions bud, the Gag polyproteins are cleaved by the viral protease into the three major viral structural proteins, matrix (MA, p17), capsid (CA, p24), and nucleocapsid (NC, p7), as well as three smaller peptide fragments (p1, p2, p6). These proteins subsequently undergo a major rearrangement, termed maturation, wherein the CA molecules condense to form the conical core particle that encapsidates the RNA-NC ribonucleoprotein complex, and the matrix proteins form a shell that remains associated with the inner face of the viral membrane (Gelderblom, 1991; Höglund et al., 1992; Marx et al., 1988). Genetic analyses indicate that the matrix shell helps to anchor the transmembrane envelope protein (TM, gp41) on the surface of the virion, because mutations in both MA (Dorfman et al., 1994; Freed et al., 1994, 1995; Freed & Martin, 1996; Wang et al., 1993; Wang & Barklis, 1993; Yu et al., 1992) and the intraviral domain of TM (Freed & Martin, 1995, 1996; Mammano et al., 1995; Yu et al., 1993) can produce envelope-deficient virions.

HIV-1 MA also appears to perform essential functions both early and late in the viral life cycle. Prior to budding, the matrix domain of Gag directs virion assembly to the plasma membrane. Mutations in the amino terminal two-thirds of the matrix sequence can abolish or impair localization, assembly, and budding of the immature virion (Bennett et al., 1993; Bryant & Ratner, 1990; Chazal et al., 1994; Fäcke et al., 1993; Freed et al., 1990, 1994, 1995; Freed & Martin, 1995; Gheysen et al., 1989; Göttlinger et al., 1989; Shoji et al., 1990; Spearman et al., 1994; Wang et al., 1993; Wang

Reprint requests to: M. F. Summers, HHMI and Department of Chemistry and Biochemistry, University of Maryland Baltimore County, Room 122A, Chemistry-Physics Building, 1000 Hilltop Circle, Baltimore, Maryland 21228; e-mail: summers@hhmi.umbc.edu.

[3]Present address: Memorial Sloan Kettering Cancer Institute, 1275 York Avenue, New York, New York 10021.

This article is based on the DuPont Merck Young Investigator Award lecture presented by Dr. Summers at the Tenth Annual Symposium of The Protein Society in San Jose, California, on August 5, 1996

Abbreviations: HMQC-NOESY, heteronuclear multiple quantum coherence-nuclear Overhauser effect spectroscopy; NMR, nuclear magnetic resonance.

& Barklis, 1993; Wills et al., 1991; Yuan et al., 1993; Zhou et al., 1994). HIV-1 Gag associates with the membrane via an amino-terminal myristoyl modification (Bryant & Ratner, 1990; Göttlinger et al., 1989) and through ionic interactions between basic residues in the matrix domain and the acidic membrane surface (Bennett et al., 1993; Ehrlich et al., 1996; Freed et al., 1995; Wills et al., 1991; Yuan et al., 1993; Zhou et al., 1994; P. Cannon, pers. comm.).

When a new host cell is infected, the HIV-1 matrix protein appears to assist in transporting the preintegration complex to the cell nucleus. This process is mediated by a nuclear localization signal that has been mapped to a set of basic residues located near the amino terminus of HIV-1 MA (Bukrinsky et al., 1993; von Schwedler et al., 1994). It has additionally been reported that C-terminal phosphorylation of a small subset of matrix proteins allows them to associate with the integrase protein and thereby target the preintegration complex to the nuclear pore (Gallay et al., 1995a, 1995b, 1996), although several aspects of this model remain controversial (Schuitemaker et al., 1994; Freed & Martin, 1994, 1995; Bukrinskaya et al., 1996; E.O. Freed, pers. comm.).

Our laboratories have focused on structural studies of the retroviral Gag proteins to gain insights into the processes of virion assembly and disassembly, and to provide information necessary for the rational development of therapeutic agents designed to interfere with these functions. We recently determined the solution- (Massiah et al., 1994) and solid-state (Hill et al., 1996) structures of the HIV-1 matrix protein. Structures of the HIV-1 and simian immunodeficiency virus (SIV) matrix proteins were also determined independently by NMR (Matthews et al., 1994, 1995) and X-ray crystallographic methods (Rao et al., 1995), respectively. With our more recent structure determination of the amino-terminal core domain of the HIV-1 capsid protein in solution- (Gitti et al., 1996) and solid-states (Gamble et al., 1996, Momany et al., 1996), structural information is now available for each of the major Gag gene products (Fig. 1).

In this paper, we compare the three-dimensional structures of the monomeric (solution-state) and trimeric (solid-state) forms of the HIV-1 matrix protein determined in our laboratories. Although the structures are very similar, small but significant differences have been observed that offer new insights into conformational changes that may be required for virion assembly and disassembly.

Results and discussion

Refinement of the NMR structure

In our original NMR studies of the HIV-1 matrix protein, severe overlap of side chain ^{1}H and ^{13}C signals precluded efforts to unambiguously define the conformation of five amino acid residues (Pro 48–Glu 52), even though strong $NH_{(i)}$ to $NH_{(i+1)}$ nu-

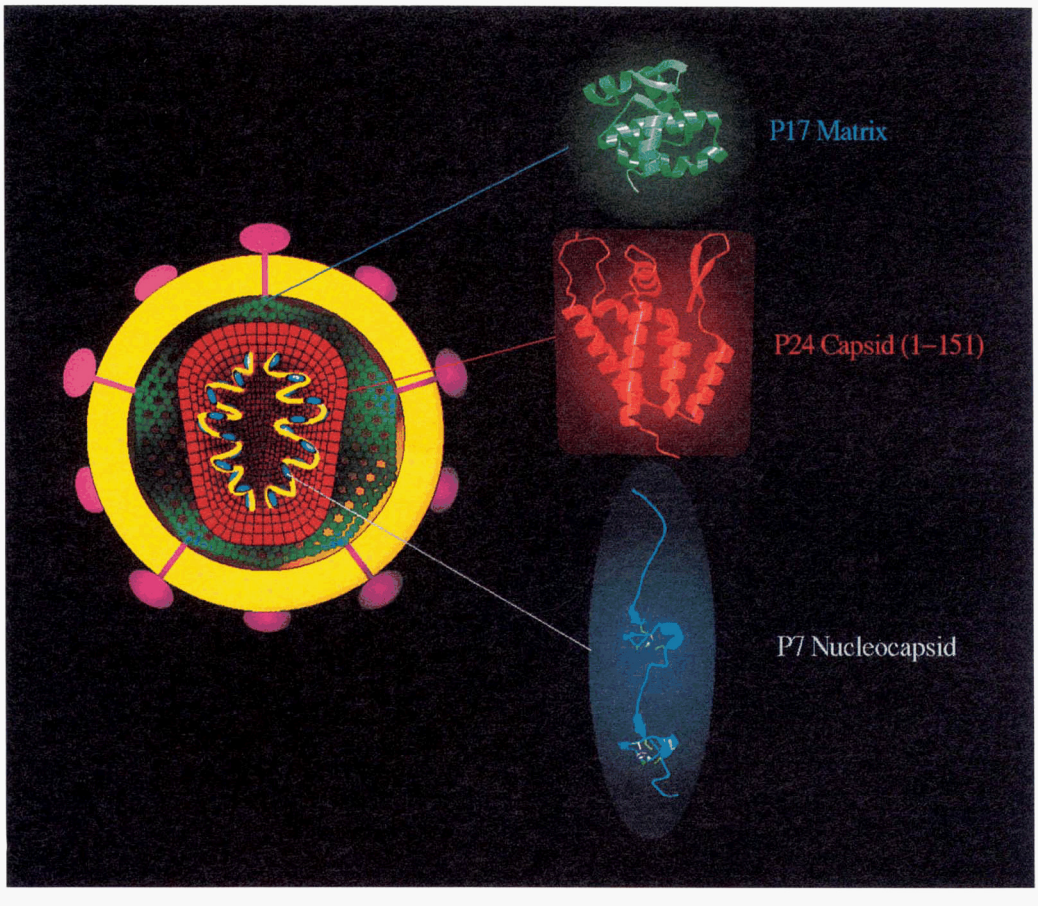

Fig. 1. Representation of the HIV-1 virion showing the relative locations of the three major Gag gene products, matrix (MA), capsid (CA), and nucleocapsid (NC) proteins. Three-dimensional solution structures of the monomeric forms of MA and NC and of the amino-terminal core domain of CA (151 residues) are shown at the right.

clear Overhauser effects (NOEs) were observed. For example, the resonances for the side-chain protons of Leu 50 and Leu 51 were indistinguishable in the three-dimensional ^{15}N-edited and three-dimensional ^{13}C-edited NOESY spectra, and significant side-chain signal overlap was observed for several nearby residues, including Leu 41, Val 46, and Ile 60. Because unambiguous assignment of interresidue side-chain NOEs could not be made using the original data, restraints for residues Pro 48-Glu 52 were not included in the early models (see Figs. 7 and 10 of Massiah et al., 1994). Spectral resolution was improved by the subsequent collection of three-dimensional ^{13}C-edited NOESY data with extensive folding in the ^{13}C dimension ($\pm$11.05 ppm with the ^{13}C carrier set at 40 ppm); and with the use of "distance filtering" (i.e., assignment of otherwise ambiguous NOE crosspeaks on the basis of interproton distances observed in the NMR structures), it was possible to assign interresidue side-chain NOEs for residues Leu 41, Val 46, Ile 60, Leu 50, and Leu 51. The new NOE data indicated a single helical turn for residues Pro 48–Glu 52 that was consistent with the earlier observation of $NH_{(i)}$–$NH_{(i+1)}$ NOE cross peaks (Massiah et al., 1994). The presence of Pro 48-αH to Leu 50-NH and Gly 49-αH to Leu 51-NH NOEs indicated that the turn contains 3_{10} helical character, as was also observed in the X-ray structures of the HIV-1 (Hill et al., 1996) and SIV (Rao et al., 1995) matrix proteins, but not in the refined NMR structure of the HIV-1 matrix protein of Matthews and co-workers (Matthews et al., 1994, 1995).

A total of 309 additional NOE-derived distance restraints were identified using the highly folded three-dimensional ^{13}C-edited NOESY data, and the original MA models were subsequently refined using a total of 908 distance restraints, corresponding to an average of 17 restraints per restrained residue. The penalties of the final twenty structures ranged from 0.14 Å^2 to 0.23 Å^2, with individual distance violations of $\leq$0.03 Å. Superposition of the Cα atoms of helices I–V and the three-stranded β-sheet afforded pairwise RMS deviations (RMSDs) of 0.57 $\pm$ 0.10 Å (Table 1). Superposition of the Cα atoms of all residues from Ser 9 to Ile 104, including the partially-ordered three-stranded mixed β-sheet, gave pairwise RMSDs of 1.16 $\pm$ 0.35 Å. The original and refined structures compare equally well with the X-ray structures, with superposition of the helical and β-sheet elements affording pairwise RMSDs of 1.54 $\pm$ 0.10 Å and 1.55 $\pm$ 0.06 Å, respectively. Coordinates for the 20 refined NMR models were deposited in the Brookhaven Protein Data Bank in April 1995 (Brookhaven ID = 2HMX).

X-ray crystal structures

Both monoclinic ($P2_1$) and hexagonal ($P6_122$) crystal forms of the HIV-1 matrix protein were determined and the structures were shown to be essentially identical (Hill et al., 1996). The monoclinic crystal form was refined at 2.3 Å resolution and is the only structure discussed here in detail. This crystal form contains two independent trimers in the asymmetric unit and all six individual matrix molecules adopt the same structure, except for variations in the length of the C-terminal helix. Superposition of the backbone Cα atoms of the six X-ray models (residues 7–104) affords pairwise RMSDs in the range 0.29–0.79 Å and an overall RMSD of 0.47 $\pm$ 0.08 Å (Table 1).

Several lines of evidence suggest that matrix is likely to be trimeric when bound to the viral membrane. First, all known matrix crystal forms contain the same trimer, suggesting that this is the preferred matrix packing arrangement at high concentrations, as in the virion. Matrix trimers were observed in three different HIV-1 matrix crystal forms (Hill et al., 1996), and an analogous trimer was also observed in the crystal structure of SIV matrix (Rao et al., 1995). The trimeric structure is also highly compatible with membrane binding because all of the individual basic residues implicated in acidic membrane binding cluster on one surface of the trimer (P. Cannon, pers. comm.; Freed et al., 1994). Moreover, when this cationic surface is oriented toward the viral membrane, all of the matrix C termini project away from the opposite side of the trimer, as if toward the center of the virion. This orientation seems reasonable because the matrix C termini are initially linked to the N termini of the internal capsid protein in the Gag precursor.

Comparison of the X-ray and NMR models

The detailed comparison described here is for the HIV-1 MA structures determined in our laboratories (Massiah et al., 1994; Hill et al., 1996). However, for completeness we have also examined the other NMR structure of HIV-1 MA (Matthews et al., 1994, 1995) and the crystal structure of the SIV MA trimer (Rao et al., 1995), which were determined elsewhere (see Table 1). We note that the 1.55 $\pm$ 0.06 Å RMSD reported in Table 1 for superposition of our HIV-1 MA NMR model (Massiah et al., 1994) with the SIV MA crystal structure (Rao et al., 1995) corrects an erroneous report that these two matrix structures align with an RMSD of 3.67 Å (Matthews et al., 1996). This error was due to incorrect alignment of the amino acid sequences of the two proteins (S. Matthews, pers. comm.).

As reported previously (Hill et al., 1996), the NMR and X-ray models of the HIV-1 matrix protein exhibit highly similar three-dimensional folds. Superposition of the backbone Cα atoms of residues Ser 9–Ile 104 affords pairwise RMSDs of 1.93 $\pm$ 0.27 Å. A better fit is obtained when residues of the exposed, partially ordered β-hairpin (residues Arg 22–Lys 30) and the extended, partially ordered segment that connects helices IV and V (Ile 92–Val 95) are not included in the fitting (RMSD = 1.55 $\pm$ 0.06 Å). The only major difference between the NMR and X-ray models involves the relative length of the C-terminal helix (helix V). Helix V terminates at Gln 108 in the NMR models and in one of the X-ray models, but is extended by up to 14 additional residues in the other X-ray models. NOE and chemical shift analyses performed for the monomeric protein in solution at 35 °C indicated that residues Asn 109–Thr 122 are disordered (Massiah et al., 1994), and it is possible that crystallization conditions (4 °C) favored the observed helical conformations. In addition, intermolecular packing interactions between the C-terminal helices of two of the six matrix molecules in the asymmetric unit probably extend the length of these helices. In both the NMR and X-ray structures, Ile 104 is the last MA residue that contacts the rest of the globular protein core. In the X-ray structure of SIV MA, helix V similarly terminates at Leu 108, but subsequent residues Val 110–Thr 117 form a β-hairpin (Rao et al., 1995).

The above differences involve residues beyond the globular core domain of HIV-1 MA. Comparison of the NMR and X-ray models of the protein core reveals a single significant structural difference that involves an approximately 6 Å displacement of the 3_{10} helix comprising residues Pro 66–Gly 71. Excluding this 3_{10} helix from the superposition calculations results in a significant decrease of the RMSD (from 1.55 $\pm$ 0.006 Å to 1.37 $\pm$ 0.06 Å; Table 1 and Fig. 2). Displacement of the 3_{10} helix results from subtle differences in the backbone torsion angles of Pro 66, coupled with

Table 1. *Comparison of HIV-1 and SIV matrix protein structures*

A. Relative convergence of our HIV-1 MA NMR and X-ray structures (Å)

Backbone Cα	Superposition of 2HMX NMR models [Massiah et al. (1994)][a]	Superposition of the six X-ray models [Hill et al. (1996)][b]
All α-helices + β-sheet[c]	0.57 ± 0.10	0.44 ± 0.10
Above + 3_{10} helix and turns[d]	0.57 ± 0.10	0.43 ± 0.08
Ser 9–Ile 104	1.16 ± 0.35	0.47 ± 0.08
All atoms		
All helices + β-sheets	1.74 ± 0.13	1.20 ± 0.16

B. Comparison of all HIV-1 NMR structures with the X-ray structures

Backbone Cα	Massiah et al. (1994) 20 NMR models 2HMX versus X-ray	Matthews et al. (1994) 1TAM NMR model versus X-ray[e]
All α-helices	1.26 ± 0.06	2.12 ± 0.05
Above + β-sheet & turns	1.37 ± 0.06	2.30 ± 0.04
Above + 3_{10} helix	1.55 ± 0.06	2.27 ± 0.04
Ser 9–Ile 104	1.93 ± 0.27	2.70 ± 0.03

C. Comparison of all HIV-1 structures with the SIV structure

Backbone Cα	Hill et al. (1996) X-ray versus SIV X-ray[f]	Massiah et al. (1994) 2HMX NMR versus SIV X-ray[f]	Matthews et al. (1996) 1TAM NMR versus SIV X-ray[f]
All α-helices	0.50 ± 0.05	1.24 ± 0.07	2.19
Above + β-sheet and turns	0.50 ± 0.05	1.38 ± 0.07	2.37
Above + 3_{10} helix	0.50 ± 0.05	1.55 ± 0.06	2.34
Ser 9–Ile 104	0.59 ± 0.06	1.85 ± 0.23	2.68

D. Comparison of the HIV-1 MA NMR structures

Backbone Cα	Massiah et al. (1994) (1HMX) versus Matthews et al. (1996) (1TAM)	Massiah et al. (1994) (2HMX) versus Matthews et al. (1996) (1TAM)
All α-helices	2.12 ± 0.12	2.09 ± 0.09
All α-helices + β-sheet	2.13 ± 0.12	2.11 ± 0.09
Above +3_{10} helix	2.12 ± 0.11	2.17 ± 0.07
Ser 9–Ile 104	2.59 ± 0.16	2.69 ± 0.10

[a]RMSDs were calculated for the 20 refined 2HMX NMR structures.

[b]The RMSDs of the X-ray structures were calculated from the six independently generated models.

[c]All α-helices = helices I (Ser 9–Glu 17); II (Lys 30–Phe 44); III (Thr 53–Gln 65); IV (Ser 72–Ile 92); V (Asp 95–Ile 104). Including β-sheet: Ser 9–Leu 21, Gln 28–Phe 44.

[d]The 3_{10} helix spans residues Pro 66–Gly 71.

[e]Coordinates for only one low penalty refined MA NMR structure by Matthews et al. (1996) were available from the Brookhaven Protein Data Bank (1TAM).

[f]Coordinates for the SIV trimers were kindly provided by Dr. Zihe Rao and Prof. David Stuart (Oxford, UK).

significant differences in the backbone ψ angle of Gly 71 (148 degrees and −80 degrees in the X-ray and NMR structures, respectively) and the ϕ angle of Ser 72 (−73 degrees and −179 degrees in the X-ray and NMR structures, respectively).

Detailed examination of the crystallographic and NMR data have confirmed that the respective models are correct and genuinely differ in this region. As shown in Figure 3, the crystal model fits the unbiased multiple isomorphous displacement (MIR)/ averaged density in this region and is also consistent with simulated annealing omit maps (not shown). To evaluate the NMR models, the Leu 68 and Tyr 79 side-chain protons and the Ser 72 backbone amide proton served as useful reporters. As shown in Figure 4, the side chain of Leu 68 (located on the 3_{10} helix) is in close proximity to the Tyr 79 aromatic ring (located on helix IV). In the X-ray structures, the Leu 68-Hγ proton is approximately equidistant from the Tyr 79-Hδ (4.17 Å) and Hε (4.44 Å) protons,

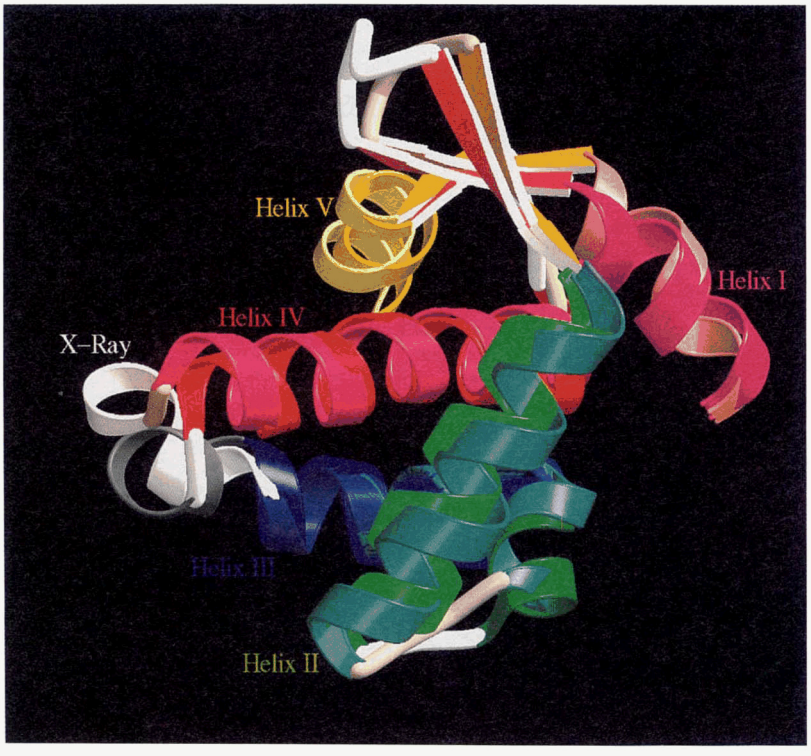

Fig. 2. Superposition of the HIV-1 matrix protein structures, determined by NMR (darker shades) and X-ray crystallography, showing the 6 Å displacement of the 3_{10} helix (residues Pro 66–Gly 71). This helix makes intermolecular contacts in the trimer, which suggests that the observed differences reflect actual conformational changes that occur during virus assembly and disassembly. The figure was generated by superposition of the backbone Cα atoms of residues Ser 9–Glu 17, Lys 30–Phe 44, Pro 48–Glu 52, Thr 53–Gln 65, Ser 72–Ile 92, and Lys 95–Ile 104, and displayed using the Molscript (Kraulis, 1991) and Raster-3D (Bacon & Anderson, 1988) software packages.

whereas in the NMR models, the –Leu 68-Hγ proton is significantly closer to the Tyr 79-Hδ proton (3.65 Å) than to the Tyr 79-Hϵ proton (4.87 Å). Thus, NOE crosspeaks involving these protons should allow discrimination between the NMR and X-ray models. As shown in Figure 5A, the Leu 68-Hγ proton exhibits a strong-intensity NOE crosspeak with the Tyr 79-Hδ aromatic proton, but only a weak signal to the Tyr 79-Hϵ proton. In addition the Leu 68-$^{\delta 1}CH_3$ (pro-R) diastereotopic methyl group exhibits strong intensity NOE crosspeaks with the Tyr 79-Hδ proton and only weak crosspeaks with the Tyr 79-Hϵ proton, whereas the Leu 68-$^{\delta 2}CH_3$ (pro-S) methyl exhibits strong NOE crosspeaks to the Tyr 79-Hβ protons (not shown). Finally, as shown in Figure 5B, the backbone NH proton of Ser 72 exhibits strong-intensity NOEs to the Gly 71-NH and Leu 75-$^{\delta}CH_3$ protons, consistent with the short interproton distances of 2.7 Å and 3.3 Å, respectively, in the NMR model, but seemingly inconsistent with the distances of

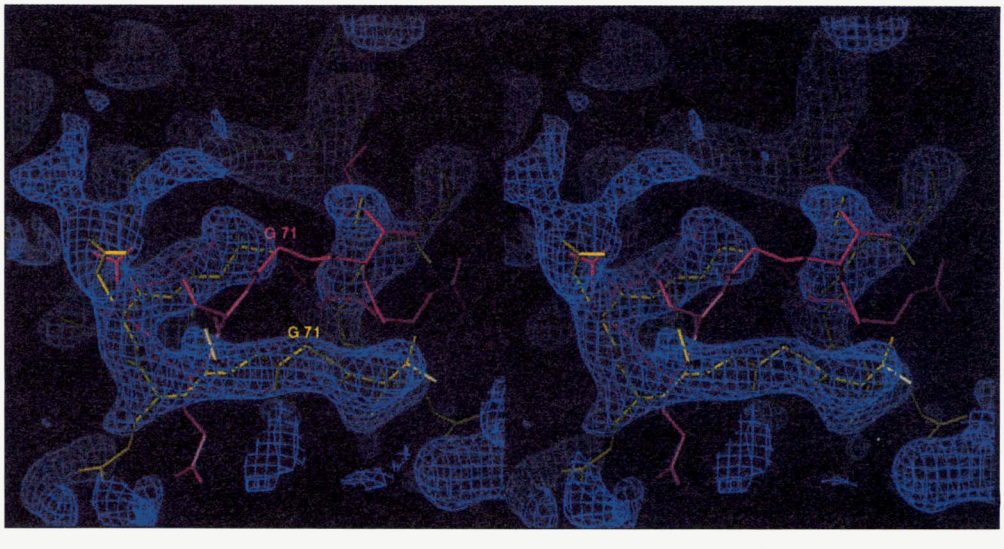

Fig. 3. Unbiased electron density map contoured at 1.2 Å RMSD. MIR phases calculated to 2.5 Å resolution were refined by six-fold non-crystallographic symmetry averaging, solvent flattening, and histogram shifting with the program DM (Cowtan, 1994). An alpha carbon superposition of the current refined X-ray (yellow) and NMR (magenta) structures is shown. Gly 72 is labeled for both models and Pro 66 is visible at the right hand edge of this figure. This figure was made with the program O (Jones et al., 1991).

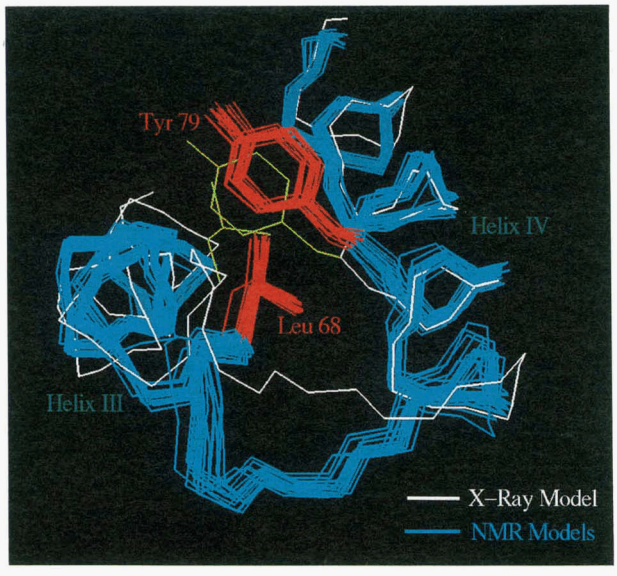

Fig. 4. Best fit superposition of the backbone heavy atoms of residues Thr 53 to Gln 65 and Ser 72 to Gln 90 of the 20 refined NMR structures (blue), compared with a representative X-ray crystal structure model (white), showing that the relative positions of the Tyr 79 and Leu 68 side chains are different in the NMR and X-ray models. The side chains of Leu 68 and Tyr 79 are colored red in the NMR models, and green (Tyr 79) and yellow (Leu 68) in the X-ray models.

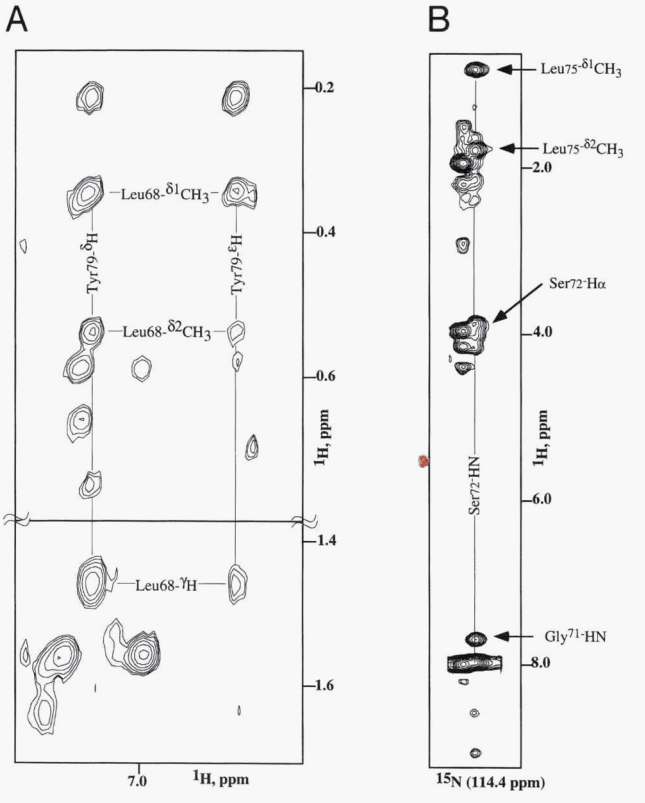

Fig. 5. **A**: Portion of the two-dimensional NOESY spectrum obtained for the HIV-1 matrix protein (120 ms mixing time) showing NOE crosspeaks involving aromatic side-chain protons. Correlations between Tyr 79-Hδ and Hε protons and the methyl protons of Leu 68 are labeled. The Leu 68-$^{\delta 1}CH_3$ methyl protons exhibit a stronger intensity NOE crosspeak to Tyr 79-Hδ protons than to Hε protons. In addition, Leu 68-Hγ exhibits a very strong NOE crosspeak with the Tyr 79-Hδ protons, but only a weak cross peak with the Tyr 79-Hε protons. **B**: Strip from the three-dimensional ^{15}N-NOESY-HSQC spectrum obtained for ^{15}N-labeled MA showing NOE correlations from the Ser 72 backbone amide proton to the Gly 71 backbone amide and Leu 75-δCH_3 methyl protons. These NOE data are consistent with the orientation of the 3_{10} helix observed in the NMR models, but are incompatible with the X-ray model.

4.6 Å and 5.6 Å, respectively, in the X-ray models. To address the possibility that the NOE and X-ray data could be simultaneously satisfied, combined simulated annealing refinement was performed against both the X-ray data and the Ser 72-NH to Gly 71-NH and to Leu 75-$^{\delta}CH_3$ NOE distance restraints (Brünger, 1992). Three separate trajectories were performed, yielding average distances for the Ser 72-NH to Gly 71-NH and to Leu 75-$^{\delta}CH_3$ distances of 4.5 Å and 5.3 Å, respectively. The minimum values observed over all 18 models in these calculations were 4.4 Å and 4.3 Å, providing clear evidence that the differences observed in the NMR and X-ray models reflect actual structural differences between the monomeric and trimeric forms of the protein.

A second, smaller difference between the NMR and X-ray MA models occurs at the C-terminal end of helix II, with the largest deviation observed for residue Ala 45 (approximately 1 Å). Analysis of NOE intensities suggests that this difference is real. However, because Ala 45 is positioned at the terminus of helix II and does not make long-range intramolecular contacts, and because predicted differences in local interproton distances are small, it is not possible to unambiguously discriminate between the X-ray and NMR models on the basis of the NOE data.

Differences between the solution and crystal structures arise as a consequence of matrix trimerization in the crystal. The trimer interface is created primarily by packing of the C terminus of helix II and its adjacent loop (residues 42–47) against the 3_{10} helix and the following loop (residues 69–74). Thus, the residues exhibiting the largest differences between the solution and crystal structures reside at the center of this interface. In particular, Thr 70-O and Ser 72-N both make intermolecular hydrogen bonds to Asn 47-N and Ala 45-O. The Ala 45 methyl group also makes hydrophobic interactions across the interface. These interactions serve to rotate the Ser 72 amide nitrogen toward the trimer interface and displace Ala 45 into the interface.

The fact that the 3_{10} helix undergoes a 6 Å displacement upon MA protein trimerization raises the intriguing possibility that this structural change may be required for assembly and disassembly of the matrix shell. Interestingly, both terminal residues of the 3_{10} helix (Pro 66 and Gly 71) are highly conserved among 96 published strains of HIV-1 (Meyers et al., 1995). Pro 66 serves as a bridge between helix III and the 3_{10} helix, and may provide the flexibility necessary to allow the 3_{10} helix to reorient. This proline is only sparingly substituted by serine (Meyers et al., 1995), and it is interesting that a serine residue was also found to bridge α- and 3_{10}-helical substructures in the HIV-1 capsid protein (Gitti et al., 1996). Conservation of Gly 71 at the other end of the 3_{10} helix may help to facilitate the large torsion angle changes associated with this residue since glycine lacks a side chain.

In summary, we have documented a 6 Å displacement of the 3_{10} helix comprising residues Pro 66–Gly 71 in the X-ray and NMR structures of the HIV-1 matrix protein. Conserved residues Pro 66 and Gly 71 appear to function as hinges that allow the 3_{10} helix to reorient on trimerization, and this reorientation may be important for protein–protein interactions associated with viral assembly and disassembly.

Materials and methods

Recombinant HIV-1 matrix proteins used in both X-ray and NMR studies were expressed and purified using identical procedures (Massiah et al., 1994). The highly-folded three-dimensional ^{1}H-, ^{13}C-edited NOESY spectrum (150 msec mixing time) of the original, uniformly ^{13}C, ^{15}N-labeled protein sample (5.6 mM) was obtained with a General Electric PSG OMEGA-600 NMR spectrometer (599.71 MHz, ^{1}H). The data were acquired with 32 transients per hypercomplex t_1, t_2 pair, a ^{13}C dwell of 300 μs ($\pm$11.05 ppm with the ^{13}C carrier set at 40 ppm), and acquisition times of 22 ms (^{1}H, t_1, 256*), 13.5 ms (^{13}C, t_2, 90*) and 112.6 ms (^{1}H, t_3, 1,024 points).

Previously generated MA NMR structures (1HMX) were refined using DSPACE (Biosym, Inc., San Diego, CA). Conjugate gradient minimization (CGM) and moderate-temperature simulated annealing was only performed for residues Val 7 to Gln 108 because no experimental distance restraints were employed for the remaining residues. Structures were initially treated with several cycles of 64–128 steps of local simulated annealing and minimization, followed by global CGM.

Acknowledgments

Financial support from the NIH (AI30917 to MFS, AI37524 to WIS and CPH) and the Lucille P. Markey Charitable Trust is gratefully acknowledged. We thank Tom O'Hern (HHMI-UMBC) for technical support and for generating Figure 1.

References

Bacon DJ, Anderson WF. 1988. A fast algorithm for rendering space-filling molecule pictures. *J Mol Graph 6*:219–220.

Bennett RP, Nelle TD, Wills JW. 1993. Functional chimeras of the Rous sarcoma virus and human immunodeficiency virus gag proteins. *J Virol 67*:6487–6498.

Brünger AT. 1992. X-PLOR, a system for crystallography and NMR. Version 3.1. Yale University, New Haven, CT: Yale University Press.

Bryant M, Ratner L. 1990. Myristoylation-dependent replication and assembly of human immunodeficiency virus 1. *Proc Natl Acad Sci USA 87*:523–527.

Bukrinskaya AG, Ghorpade A, Heinzinger NK, Smithgall TE, Lewis RE, Stevenson M. 1996. Phosphorylation-dependent human immunodeficiency virus type 1 infection and nuclear targeting of viral DNA. *Proc Natl Acad Sci USA 93*:367–371.

Bukrinsky MI, Haggerty S, Dempsey MP, Sharova N, Adzhubei A, Spitz L, Lewis P, Goldfarb D, Emerman M, Stevenson M. 1993. A nuclear localization signal within HIV-1 matrix protein that governs infection of non-dividing cells. *Nature 365*:666–669.

Chazal N, Carrière C, Gay B, Boulanger P. 1994. Phenotypic characterization of insertion mutants of the human immunodeficiency virus type 1 Gag precursor expressed in recombinant baculovirus-infected cells. *J Virol 68*:111–122.

Cowtan KD. 1994. An automated procedure for phase improvement by density modification. *Joint CCP4 and ESF-EACBM Newsletter 31*:34–38.

Dorfman T, Mammano F, Haseltine WA, Göttlinger HG. 1994. Role of the matrix protein in the virion association of the human immunodeficiency virus type 1 envelope glycoprotein. *J Virol 68*:1689–1696.

Ehrlich LS, Fong S, Scarlata S, Zybarth G, Carter C. 1996. Partitioning of HIV-1 Gag and Gag-related proteins to membranes. *Biochemistry 35*:3933–3943.

Fäcke M, Janetzko A, Shoeman RL, Kräusslich H-G. 1993. A large deletion in the matrix domain of the human immunodeficiency virus Gag gene redirects virus particle assembly from the plasma membrane to the endoplasmic reticulum. *J Virol 67*:4972–4980.

Freed EO, Englund G, Martin AM. 1995. Role of the basic domain of human immunodeficiency virus type 1 matrix in macrophage infection. *J Virol 69*:3949–3954.

Freed EO, Martin AM. 1996. Domains of the human immunodeficiency virus type 1 matrix and gp41 cytoplasmic tail required for envelope incorporation into virions. *J Virol 70*:341–351.

Freed EO, Martin AM. 1994. HIV-1 Infection of non-dividing cells. *Nature 369*:107–108.

Freed EO, Martin AM. 1995. Virion incorporation of envelope glycoproteins with long but not short cytoplasmic tails is blocked by specific, single amino acid substitutions in the human immunodeficiency virus type 1 matrix. *J Virol 69*:1984–1989.

Freed EO, Myers DJ, Risser R. 1990. Characterization of the fusion domain of the human immunodeficiency virus type 1 envelope glycoprotein gp41. *Proc Natl Acad Sci USA 87*:4650–4654.

Freed EO, Orenstein JM, Buckler-White AJ, Martin MA. 1994. Single amino acid changes in the human immunodeficiency virus type 1 matrix protein block virus particle production. *J Virol 68*:5311–5320.

Gallay P, Stitt V, Mundy C, Oettinger M, Trono D. 1996. Role of karyopherin pathway in human immunodeficiency virus type I nuclear import. *J Virol 70*:1027–1032.

Gallay P, Swingler S, Aiken C, Trono D. 1995a. HIV-1 infection of nondividing cells: C-terminal tyrosine phosphorylation of the viral matrix protein is a key regulator. *Cell 80*:379–388.

Gallay P, Swingler S, Song J, Bishman F, Trono D. 1995b. HIV nuclear import is governed by the phosphotyrosine-mediated binding of matrix to the core domain of integrase. *Cell 83*:569–576.

Gamble TR, Vajdos F, Yoo S, Worthylake DK, Houseweart SM, Sundquist WI, Hill CP. 1996. Crystal structure of human cyclophilin A bound to the amino-terminal domain of the HIV-1 capsid. *Cell*, in press.

Gelderblom HR. 1991. Assembly and morphology of HIV: Potential effect of structure on viral function. *AIDS 5*:617–637.

Gheysen D, Jacobs E, de Foresta F, Thiriart C, Francotte M, Thines D, De Wilde M. 1989. Assembly and release of HIV-1 precursor $Pr55^{gag}$ virus-like particles from recombinant baculovirus-infected insect cells. *Cell 59*:103–112.

Gitti RK, Lee BM, Walker J, Summers MF, Yoo S, Sundquist WI. 1996. Structure of the amino-terminal core domain of the HIV-1 capsid protein. *Science 273*:231–235.

Göttlinger HG, Sodroski JG, Haseltine WA. 1989. Role of capsid precursor processing and myristoylation in morphogenesis and infectivity of human immunodeficiency virus type 1. *Proc Natl Acad Sci USA 86*:5781–5785.

Hill CP, Worthylake D, Bancroft DP, Christensen AM, Sundquist WI. 1996. Crystal structures of the trimeric HIV-1 matrix protein: Implications for membrane association. *Proc Natl Acad Sci USA 93*:3099–3104.

Höglund S, Öfverstedt L-G, Nilsson Å, Lundquist P, Gelderblom H, Özel M, Skoglund U. 1992. Spatial visualization of the maturing HIV-1 core and its linkage to the envelope. *AIDS Research and Human Retroviruses 8*:1–7.

Jones TA, Zou J, Cowan SW, Kjeldgaard M. 1991. Improved methods for building protein models in electron density maps and location of errors in these models. *Acta Crystallogr A47*:110–119.

Kraulis PJ. 1991. MOLSCRIPT: A program to produce both detailed and schematic plots of protein structures. *J Appl Crystallogr 24*:946–950.

Mammano F, Kondo E, Sodroski J, Bukovsky A, Gottlinger HG. 1995. Rescue of human immunodeficiency virus type I matrix protein mutants by envelope glycoproteins with short cytoplasmic domains. *J Virol 69*:3824–3830.

Marx PA, Munn RJ, Joy KI. 1988. Computer emulation of thin section electron microscopy predicts an envelope-associated icosadeltahedral capsid for human immunodeficiency virus. *Lab Invest 58*:112–118.

Massiah MA, Starich MR, Paschall C, Summers MF, Christensen AM, Sundquist WI. 1994. Three dimensional structure of the human immunodeficiency virus type 1 matrix protein. *J Mol Biol 244*:198–223.

Matthews S, Barlow P, Boyd J, Barton G, Russell R, Mills H, Cunningham M, Meyers N, Burns N, Clark N, Kingsman S, Kingsman A, Campbell I. 1994. Structural similarity between the p17 matrix protein of HIV-1 and interferon-γ. *Nature (London) 370*:666–668.

Matthews S, Barlow P, Clark N, Kingsman S, Kingsman A, Campbell I. 1995. Refined solution structure of p17, the HIV matrix protein. *Biochem Soc Trans 23*:725–728.

Meyers G, Korber B, Hahn BH, Jeang K-T, Mellors JW, McCutchan FE, Henderson LE, Pavlakis GN, eds. 1995. *Human Retroviruses and AIDS*. Los Alamos, NM: Los Alamos National Laboratory.

Momany C, Kovari LC, Prongay AJ, Keller W, Gitti RK, Lee BM, Gorbalenya AE, Tong L, McClure J, Ehrlich LS, Summers MF, Carter C, Rossmann MG. 1996. Crystal structure of dimeric HIV-1 capsid protein. *Nature Struct Biol 3*:763–770.

Rao Z, Belyaev AS, Fry E, Roy P, Jones IM, Stuart DI. 1995. Crystal structure of SIV matrix antigen and implications for virus assembly. *Nature 378*:743–747.

Schuitemaker H, Kootstra NA, Fouchier RAM, Hooibrink B, Meidema F. 1994. Productive HIV-1 infection of macrophages restricted to the cell fraction with proliferative capacity. *EMBO J 13*:5929–5939.

Shoji S, Tashiro A, Kubota Y. 1990. Antimyristoylation of gag proteins in human T-cell lymphotropic and human immunodeficiency viruses by N-myristoyl glycinal diethylacetal. *Ann NY Acad Sci 616*:97–115.

Spearman P, Wang J-J, Vander Heyden N, Ratner L. 1994. Identification of human immunodeficiency virus type 1 Gag protein domains essential to membrane binding and particle assembly. *J Virol 68*:3232–3242.

von Schwedler U, Kornbluth RS, Trono D. 1994. The nuclear localization signal of the matrix protein of human immunodeficiency virus type 1 allows the establishment of infection in macrophages and quiescent T lymphocytes. *Proc Natl Acad Sci USA 91*:6992–6996.

Wang C-T, Barklis E. 1993. Assembly, processing, and infectivity of human immunodeficiency virus type 1 Gag mutants. *J Virol 67*:4264–4273.

Wang C-T, Zhang Y, McDermott J, Barklis E. 1993. Conditional infectivity of a human immunodeficiency virus matrix domain deletion mutant. *J Virol 67*:7067–7076.

Wills JW, Craven RC, Weldon RA Jr, Nelle TD, Erdie CR. 1991. Suppression of retroviral MA deletions by the amino-terminal membrane-binding domain of $p60^{src}$. *J Virol 65*:3804–3812.

Yuan X, Yu X, Lee T-H, Essex M. 1993. Mutations in the N-terminal region of human immunodeficiency virus type I matrix protein block intracellular transport of the Gag precursor. *J Virol 67*:6387–6394.

Yu X, Yuan X, Matsuda Z, Lee T-H, Essex M. 1992. The matrix protein of human immunodeficiency virus type I is required for incorporation of viral envelope protein into mature virions. *J Virol 66*:4966–4971.

Yu X, Yuan X, McLane MF, Lee T-H, Essex M. 1993. Mutations in the cytoplasmic domain of human immunodeficiency virus type 1 transmembrane protein impair the incorporation of env proteins into mature virions. *J Virol 67*:213–221.

Zhou W, Parent LJ, Wills JW, Resh MD. 1994. Identification of a membrane-binding domain within the amino-terminal region of human immunodeficiency virus type 1 Gag protein which interacts with acidic phospholipids. *J Virol 68*:2556–2569.